Science of the Total Environment 685 (2019) 37–49

Contents lists available at ScienceDirect

Science of the Total Environment

journal homepage: www.elsevier.com/locate/scitotenv

Convenient use of electrical conductivity measurements to investigate hydrological processes in Alpine headwaters

Karina Cano-Paoli [a], Gabriele Chiogna [b,c], Alberto Bellin [a,*]

[a] Department of Civil, Environmental and Mechanical Engineering, University of Trento, via Mesiano 77, I-38123 Trento, Italy
[b] Technische Universität München. Arcisstrasse 21, 80333 München, Germany
[c] Universität Innsbruck, Institut für Geographie, Innrain 52, 6020 Innsbruck, Austria

HIGHLIGHTS

- Hydrograph separation with proper uncertainty quantification on the use of different tracers
- A new method based on compression of hysteresis loops for time lag estimation between EC and Q
- Use of EC as proxy for Q including the time lag variable

GRAPHICAL ABSTRACT

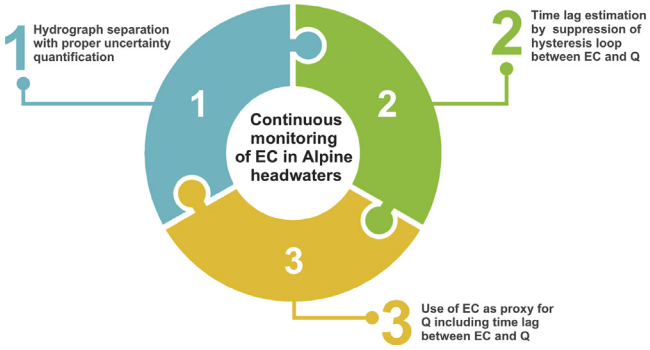

ARTICLE INFO

Article history:
Received 15 June 2018
Received in revised form 12 May 2019
Accepted 12 May 2019
Available online 20 May 2019

Editor: Damia Barcelo

Keywords:
Alpine catchment
Electrical conductivity
Hydrograph separation
Hysteresis
Time lag
Empirical relationships
Streamflow prediction

ABSTRACT

Developing effective hydrological models for streamflow generation in Alpine catchments is challenging due to the inherent complexity of the intertwined processes controlling water transfer from hillslopes to streams and along the river network. Over the past decades, studies have proposed complementing traditional hydrological information with environmental tracer data, e.g. stable isotopes or electrical conductivity (EC), for different purposes such as the separation of streamflow components or the estimation of catchment mean residence time. In particular EC has been applied in Alpine environments mainly for hydrograph separation but also, more recently, considered as a possible proxy for streamflow (Q) prediction. The reason is simple: EC data loggers are convenient because of their relative low cost, easiness of installation and low maintenance, unlike traditional water stage gauges. However, EC time series require careful interpretation since electrical conductivity is influenced by a number of geochemical processes not always introduced in the analysis since these can be difficult to parametrize. Likewise, the relationship between EC and Q is very complex because it is characterized by hysteresis loops and often site specific. This study shows how the continuous monitoring of EC in Alpine catchments can be useful specifically for: hydrograph separation, including a proper quantification of uncertainty; process understanding of catchment functioning through the interpretation of hysteresis loops and time lags between EC and Q signals; and finally, water discharge estimation through calibrated functional EC-Q relationships. We discuss advantages and limitations of the use of EC in hydrology and provide information to encourage its use in studies dealing with streamflow generation dynamics in snow-dominated catchments.

* Corresponding author.
E-mail address: alberto.bellin@unitn.it (A. Bellin).

https://doi.org/10.1016/j.scitotenv.2019.05.166

1. Introduction

In Alpine headwaters water storage is chiefly under the form of snow and ice (Kuhn and Batlogg, 1998; Stewart, 2009), yet they are characterized by a rapid response to rainfall events. In order to understand and separate processes leading to runoff generation, a number of studies have suggested supplementing traditional hydrological observations with environmental tracer data. For example, environmental tracers (e.g. oxygen-18, deuterium, ion-chloride) have been used to estimate the mean residence time (Chiogna et al., 2014; Herms et al., 2019; Jódar et al., 2016), the altitude recharge (Barberá et al., 2018), and also to perform end-member mixing analysis (Penna et al., 2014; Engel et al., 2015; Jódar et al., 2017) in glacierized catchments. Behrens et al. (1971) used multi-tracer data (tritium, deuterium, rhodamine WT and electrical conductivity) to gain a deeper understanding of the water budget in temperate glaciers. Collins (1979) analyzed the spatial and temporal variability of electrical conductivity and major cations concentration in a glacial environment, identifying diurnal cycles and hysteresis loops. Laudon and Slaymaker (1997) performed hydrograph separation of runoff events considering electrical conductivity (EC), specific concentration of silicon (Si) and the stable isotopes oxygen-18 and deuterium as hydrological tracers. The findings of these studies highlighted limits and merits of using electrical conductivity as a tracer in hydrograph separation. Brown et al. (2006) used an end-member mixing approach (considering major ions, Si and electrical conductivity) to unveil complex hydrological processes in an alpine environment. More recently, Engel et al. (2015) and Penna et al. (2014, 2016a, 2016b) used hydrograph separation and end-member mixing analysis with multiple tracers to identify spatial and temporal variations of water sources in Alpine catchments. EC measurements are commonly collected in Alpine catchments (Engel et al., 2018; Laudon and Slaymaker, 1997). Differently from other tracers, EC measurements are generally characterized by a high temporal resolution and data loggers can be easily deployed at a relatively low cost. In addition, maintenance is typically limited to regular visits to the measurement site for checking the regular functioning of the sensor, in particular when it operates in harsh conditions.

Electrical conductivity is a measure of total ionic concentration and it generally depends on hydrogeochemical processes characteristic of the catchment. Recently, Benettin and Benettin and Van Breukelen (2017) proposed a mechanistic model for extracting information on individual ion contents from electrical conductivity time series. However, in alpine environments, the large difference in ionic content, and hence in EC, between glacier, snow and rainfall water on the one side, and groundwater, on the other, is generally sufficient for a separation of water of different origins (Gurnell and Fenn, 1985) without the need of an in-depth hydrogeochemical analysis. Water discharge and EC are in an inverse relationship due to the fact that new water contributing to runoff has shorter residence time than old water and hence lower ionic content. Recent studies showed that because of these characteristics, water discharge may be inferred from EC measurements, though the estimation is hampered by non-linearities and threshold effects (see e.g., Weijs et al., 2013). Moreover, the use of EC to measure streamflow, grants more flexibility for the installation than standard water level gauges, since there are no significant constraints on the geometry of the chosen monitoring section. Hence it is attractive to investigate how effectively EC time series can be used for this purpose in headwaters where the installation of a traditional gauging station is hampered by the irregularity of the cross-section and many other factors, including installation cost and the complexity of maintenance. Using EC as environmental tracer is thus appealing, though EC time series require a careful interpretation, since they may be affected by bio-geochemical processes (Hayashi et al., 2012). Earlier works have shown that the relationship between water discharge and EC can be very complex and even vary from storm to storm and have also revealed that concentration of dissolved solutes, and therefore EC, lags behind related changes in water discharge during rainfall events (Glover and Johnson, 1974a; Walling and Foster, 1975; Walling and Webb, 1980; Walling and Webb, 1986; Zuecco et al., 2015), causing the formation of hysteresis loops, a non-linear behaviour very common in hydrology, thereby hampering the use of electrical conductivity to obtain water discharge. The time lag between EC and water discharge, and the resulting hysteresis, implies that the former propagates at a different celerity with respect to streamflow (Evans and Davies, 1998).

Understanding hysteresis between hydrological variables at the runoff event time scale and the associated time lag phenomenon can further improve our knowledge on the underlying hydrological processes in complex environments such as catchments dominated by snow and glacial dynamics. At the same time, current models for streamflow prediction using electrical conductivity data could be improved by taking into account the time lag between these two variables (Weijs et al., 2013).

This work aims at showing the advantages of measuring EC continuously in Alpine catchments. Often this information is only used for a given purpose without fully exploiting the possibilities that these data offers. With this purpose in mind, EC time series collected in the Vermigliana catchment in North-East Italy are used both in a traditional way by performing hydrograph separation, including uncertainty quantification, and water discharge estimation by means of a power law relationship, as well as for novel investigations such as interpretation of hysteresis loops and testing of a time-dependent power law relationship between EC and discharge. We show that the complementary use of EC data is an advantage both for process understanding and practical applications like streamflow estimation in alpine environments.

2. Material and methods

2.1. Study site

The Vermigliana creek is one of the main headwaters of the Noce, a tributary of the Adige river, the second longest river in Italy (Chiogna et al., 2016; Majone et al., 2016). It drains a catchment area of 78.9 km^2 with a river length of 9.5 km and mean slope of 1% at the gauging station of Vermiglio (point P2 in Fig. 1). Elevations range from 1165 m.a.s.l. to 3558 m.a.s.l. at the highest peak. Vermigliana has two main tributaries, the Presanella and Presena creeks, which are fed by two glaciers bearing the same names, with peaks at 3558 m.a.s.l. and 3069 m. a.s.l., respectively. For detailed information on the glaciers characteristics see Chiogna et al. (2014) and Meteotrentino (2011). From a geological point of view the catchment is characterized by the Tonale line, the local name of the Insubric line separating the Austroalpine domain from the Southern Alps and the Adamello batholith to the west (see Fig. 1). South of the Tonale line the most distinctive element is the Adamello-Presanella intrusive massif, which occupies most of the catchment and is composed by a number of crystalline (Permian) and metamorphic (pre-Permian) rocks with low metamorphism, since the Adamello batholith is composed of many plutons (Callegari et al., 1973). North of the Tonale line metamorphic basement rocks prevail. The Vermigliana creek flows along a deep valley over quaternary deposits which power varies between about 5 to 20 m (Piccolroaz et al., 2015). The geological map of the Autonomous Province of Trento can be downloaded from http://www.protezionecivile.tn.it.

The actual climate shows the typical characteristics of an Alpine catchment, with cold winters (mean temperature of −4.5 °C) and relatively warm summers (mean temperature of 11.6 °C). Mean annual air temperature is 3.6 °C and annual precipitation averages to 1300 mm, falling as snow from early November to April. Mean temperature and precipitation were estimated using the last 20 years records available at the Passo del Tonale (PT) meteorological station located at 1875 m. a.s.l. (point PT in Fig. 1). The catchment is nearly in pristine conditions, with a very large portion covered by forest (34.18%), nude rock (31.65%) and grassland (24.18%), a smaller percentage covered by

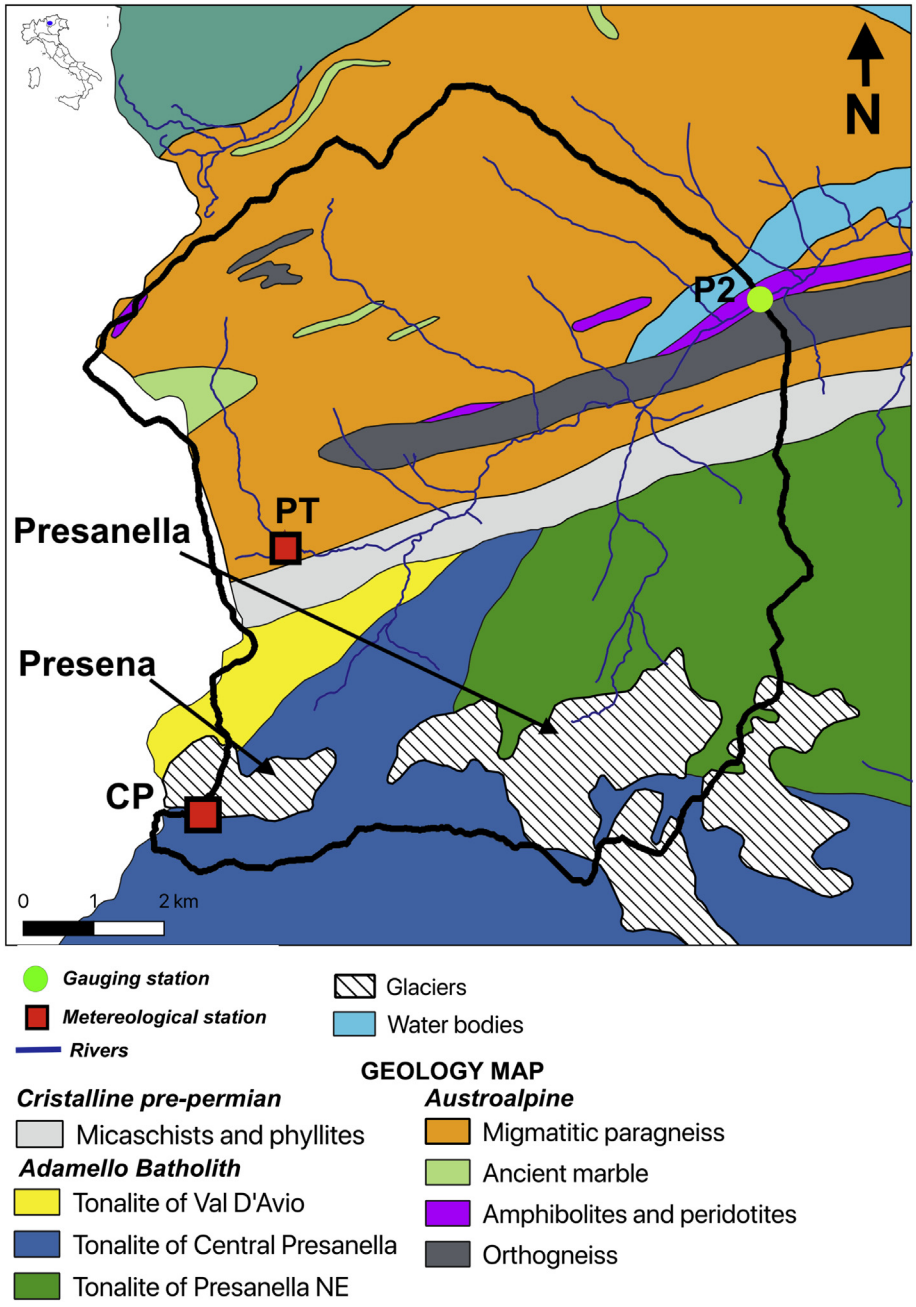

Fig. 1. Location of the monitoring stations: red squares indicate the meteorological stations of Capanna Presena (CP) and Passo del Tonale (PT) and the green dot the gauging station for continuous monitoring of streamwater discharge and electrical conductivity. The upper left inset shows the location of the catchment within the Italian territory. The catchment is superimposed to the geological map from the Autonomous Province of Trento.

glaciers (8.55%) and lakes (0.79%), while the remaining is occupied by urban areas (0.64%).

2.2. Data collection

Precipitation and air temperature at hourly resolution are available at the Passo del Tonale meteorological station and were provided by MeteoTrentino, the regional meteorological service responsible of the zone (http://www.meteotrentino.it), who also provided snow depth values at daily resolution at both PT and the Capanna Presena (CP) snow observatory. Streamwater discharge records at hourly resolution were provided by the Ufficio Dighe of the Province of Trento (http://www.floods.it) for the gauging station of Vermiglio (point P2 in Fig. 1). All meteorological and hydrological data are for the period 2011–2014.

EC was recorded at hourly resolution in the following periods: September 2011, April–November 2012, May–November 2013 and September–December 2014 by using the automatic Aqua TROLL 200 multi-parametric sensor installed at P2. The standard deviation of the measurement error is ±0.5% of the reading (+1 μS/cm when reading is <80,000 μS/cm), and the measurements are converted to specific conductance EC, referred to a standard reference temperature of 25 °C.

In addition, streamwater samples were collected at P2 during the storm event occurred on 17–21 September 2011, and hereafter referred to as R0. This task was performed using an ISCO 6712 automatic sampler, programmed to collect samples at time intervals of 4 h. A total of 19 samples were collected, stored automatically in glass vials of

300 ml and covered with Butyl-Polytetrafluorethylene (PTFE) caps. After the event, all bottles were sealed and stored in the dark to avoid potential contamination from external agents and isotopic fractionation induced by evaporation and gas-diffusion (Bolto et al., 2012) before dispatching them to the isotope laboratory of the Edmund Mach Foundation, San Michele, Trento (Italy), where stable isotopes analyses where performed for δD and $\delta^{18}O$ with an Analytical Uncertainty (AU = 1 standard deviation of reproducibility) of 2‰ and 0.2‰ respectively (Chiogna et al., 2014).

2.3. Identification of runoff events

Rainfall events were selected only when occurring during the autumn-winter season, to avoid including runoff induced by summer melting processes. During this period, baseflow conditions were in the range 1.5–2 m^3/s. In order to analyse a broad spectrum of conditions, we considered all the rainfall events >1 mm producing a water discharge peak equal or larger than 4 m^3/s. In this way, besides R0, a total of 8 runoff events were identified during the period 2012–2014 (see Fig. 2) and whose main characteristics are summarized in Table 1.

R1 and R2 correspond to runoff events generated only by rainfall in the absence of snowpack, whereas ROS1 and ROS2 have been identified as rain-on-snow events (Merz and Blöschl, 2003; Singh et al., 1997; Surfleet and Tullos, 2013). On the contrary, R5 and R6 are characterized by rainfall in presence of snowpack with no melting. For the events R3 and R4 snow data were not available due to malfunctioning of the equipment.

2.4. Uncertainty in streamflow separation

Data from event R0 were used to investigate the accuracy with which streamflow can be partitioned in pre-event and event water. The separation is performed by the two-component hydrograph separation (HS) technique (Pinder and Jones, 1969; Sklash and Farvolden, 1979) using separately three different tracers: δD, $\delta^{18}O$ and EC. Two-component HS is based on the mass balance of water and solute equations which read as follows (Sklash and Farvolden, 1979):

$$Q_{str} = Q_p + Q_e \tag{1}$$

$$C_{str}Q_{str} = C_pQ_p + C_eQ_e \tag{2}$$

where Q is streamflow [L^3/T], C [M/L^3] is tracer concentration and subscripts *str*, *p* and *e* refer to the total streamflow, pre-event and event components, respectively. Q_p and Q_e can be easily obtained from Eqs. (1) and (2) if streamflow (Q_{str}) and tracer concentration of the different components (C_{str}, C_p and C_e) are known. Yet, in order to determine Q_p and Q_e the following assumptions are needed: (1) streamflow can be approximated as the mix of two components, (2) tracer concentrations of the event and pre-event components should differ significantly, (3) tracer concentration of each component is known and, (4) surface storage contributes minimally to streamflow (Sklash and Farvolden, 1979).

Additional assumptions were made for both pre-event and event water tracer concentrations because of the lack of samples for pre-event or rainfall water during the event. Thus, we referred to data collected in the same catchment and in the same season, reported in the study by Chiogna et al. (2014). The isotopic signature of pre-event water was assumed constant (in time) and equal to $\delta D_p = -90.55‰$ and $\delta^{18}O_p = -12.60‰$, for deuterium and oxygen 18, respectively. Both were estimated as the mean value of the isotopic composition of baseflow before the onset of the rainfall. These values are consistent with grab samples collected on 9 September 2011 for the above study which showed only seasonal variability for this component. The isotopic signature of the event component was defined as the mean value for rainfall water samples collected in September 2011 and are equal to $\delta D_e = -60.00‰$ and $\delta^{18}O_e = -10.00‰$, which are consistent with the local meteoric water line (Chiogna et al., 2014). As for electrical conductivity, pre-event component was assumed constant and equal to the mean value EC_p=95.0μS/cm observed during baseflow conditions in the autumn-winter season. EC for the event water was obtained from the experimental work conducted in another catchment of the southern Alps (Penna et al., 2014), where a median value of EC_e= 8.0μS/cm (SD = 1.0μS/cm for rainfall water was obtained from a total of 65 samples). Thus, the fraction corresponding to event water (f_e) for each time step *i* can be estimated from Eqs. (1) and (2) as:

$$f_e(i) = \frac{Q_e(i)}{Q_{str}(i)} = \frac{C_{str}(i) - C_p}{C_e - C_p} \tag{3}$$

Notice that the sensor is automatically activated at the pre-selected time steps and the measurement is performed by sending an electrical current to the electrodes and measuring the resistance of the water between them. Given this configuration the error in successive measurements can be assumed as independent and normally distributed.

Considering the aforementioned assumptions, we will focus only on the uncertainty in the hydrograph separation which is produced by

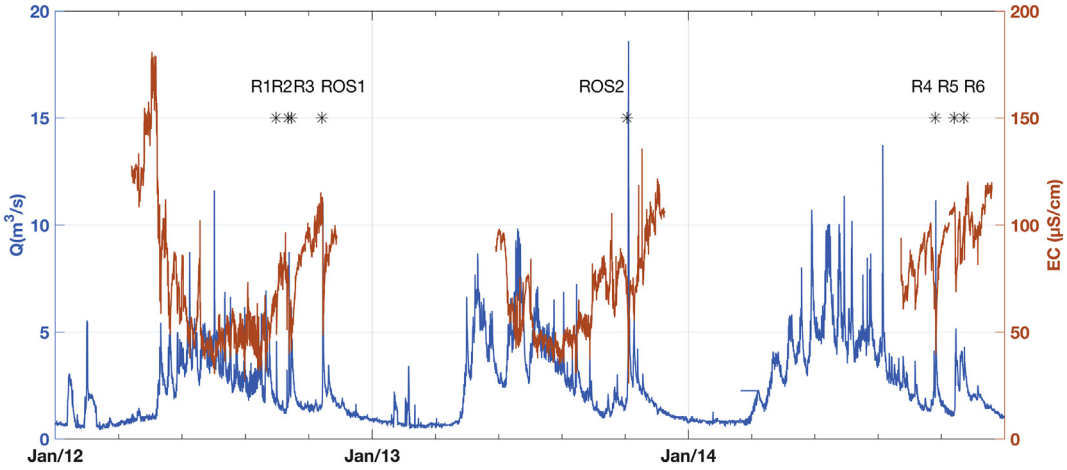

Fig. 2. Observed streamflow (blue line) and EC (orange line) at the gauging station of Vermiglio during the period 2012–2014. Black stars indicate timing of occurrence of the 8 selected runoff events.

Table 1
Main characteristics of the selected runoff events: name, date of occurrence, total rainfall recorded at PT, peak water discharge (Qmax) and variation in snow depth (ΔSD) registered at CP and PT.

Event	Date	Mean temp PT (°C)	Total rainfall PT (mm)	Qmax (m^3/s)	ΔSD at CP (cm)	ΔSD at PT (cm)
R0	17–21 Sep 2011	7.97	101.6	14.64	0	0
R1	12–14 Sep 2012	6.01	4.0	4.58	0	0
R2	26–28 Sep 2012	7.86	30.20	8.74	0	0
R3	29 Sep 2 Oct 2012	7.86	36.4	6.16	NA[a]	NA[a]
ROS1	4-7 Nov 2012	1.27	60.40	11.07	-20	-16
ROS2	22–25 Oct 2013	6.93	85.20	18.60	−8.72	−2
R4	13–15 Oct 2014	6.7	4.20	11.15	NA[a]	NA[a]
R5	4-7 Nov 2014	1.8	13.6	5.16	NA[a]	6
R6	15-16 Nov 1014	0.46	5.20	4.32	NA[a]	43

[a] NA: not available due to malfunctioning of the station.

measurement errors. Thus, assuming that the errors in the terms of Eq. (3) are independent and normally distributed, the uncertainty in f_e is given by (Genereux, 1998):

$$W_{fe}(i) = \left\{ \left[-\frac{f_e(i)}{(C_e - C_p)} W_{C_e} \right]^2 + \left[-\frac{(1-f_e(i))}{(C_e - C_p)} W_{C_p} \right]^2 + \left[\frac{1}{(C_e - C_p)} W_{C_{str}} \right]^2 \right\}^{1/2} \quad (4)$$

where W_{C_p}, W_{C_e} and $W_{C_{str}}$ are the standard deviations of the concentrations and represent the uncertainty associated to the components of tracer concentration. Given the assumption of normality for the measurement error, the 95% interval of confidence of the estimates is $f_e(i) \pm 2\, W_{fe}(i)$.

2.5. Hysteresis of EC and Q relationship at the event scale and time lag estimation

Early studies showed that the concentration of dissolved constituents may either follow or precede water discharge, with the former being the most frequent case (Glover and Johnson, 1974b; Walling and Foster, 1975). Therefore, a first intuitive definition of time lag is the difference in timing of occurrence of streamflow peak and minimum value of EC observed during the event, hereafter referred as τ_{peak}, and illustrated by the blue shaded area in Fig. 3. The resolution of the estimated lag is naturally related to measurement frequency, i.e., hourly records cannot resolve fractions of an hour.

Glover and Johnson (1974b), defined the time lag as the difference between the times at which 50% of total drop in concentration and 50% of the total increase of water discharge are observed. Hereafter this time lag is referred to as $\tau_{50\%}$ and represented by the red shaded area in Fig. 3.

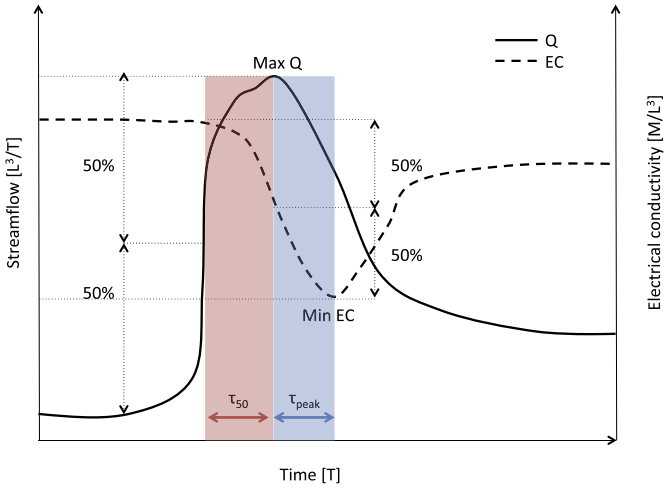

Fig. 3. Conceptual model of the time lag between streamflow and tracer during a runoff event: τ_{peak} (blue shaded area) and $\tau_{50\%}$ (red shaded area).

Here, we introduce a new definition of time lag more suitable to the use of EC as proxy of the water discharge; we identify the time lag as the shift in the EC time series needed to make the hysteresis loop as small as possible in the Q versus EC diagram. To "compress" the hysteresis loop formed during a typical runoff event such as that shown in Fig. 4a, the area inside the curve should be reduced to the minimum possible value (virtually zero), as depicted in Fig. 4c, by shifting in time the EC series of a lag τ (see Fig. 4b). After shifting *EC*, the area contained within the new hysteresis loop is computed as follows:

$$A(\tau) = \frac{1}{2} \sum_{i=1}^{n-1} \left(EC(\tau)_{i+1} + EC(\tau)_i \right) \left(Q_{i+1} - Q_i \right) \quad (5)$$

The selected time lag τ is the one that minimizes the absolute value of loop area *A* for a time series of length *n*. The absolute value is needed because depending on the direction of the hysteresis, *A* can result either positive (clockwise) or negative (counter-clockwise).

2.6. Water discharge estimates

In a first attempt to estimate *Q* from *EC* measurements we adopted the following relationships proposed by Weijs et al. (2013):

$$Q_{str}(t) = a * EC_{str}(t)^b, \quad (6)$$

$$Q_{str}(t) = a * EC_{str}(t)^b + c \quad (7)$$

and

$$Q_{str}(t) = a * \ exp(EC_{str}(t) * b), \quad (8)$$

where EC_{str} and Q_{str} are respectively the electrical conductivity and the predicted water discharge of stream water, and *a*, *b* and *c* are suitable parameters.

In addition, we propose the following new transient empirical expression:

$$Q_{str}(t) = \ exp(b * (a + TF) + c) * EC(t)^{(a+TF)} \quad (9)$$

where $TF = d \sin\left(2\pi \frac{t}{T}\right)$ is used to represent the observed hysteresis and takes into account seasonality of EC, with *d* is a model parameter to be calibrated, *T* the period and *t* the time. Successively, we will analyse the effect of taking into account the time lag by using $EC(t+\tau)$ instead of $EC(t)$in Eq. (9).

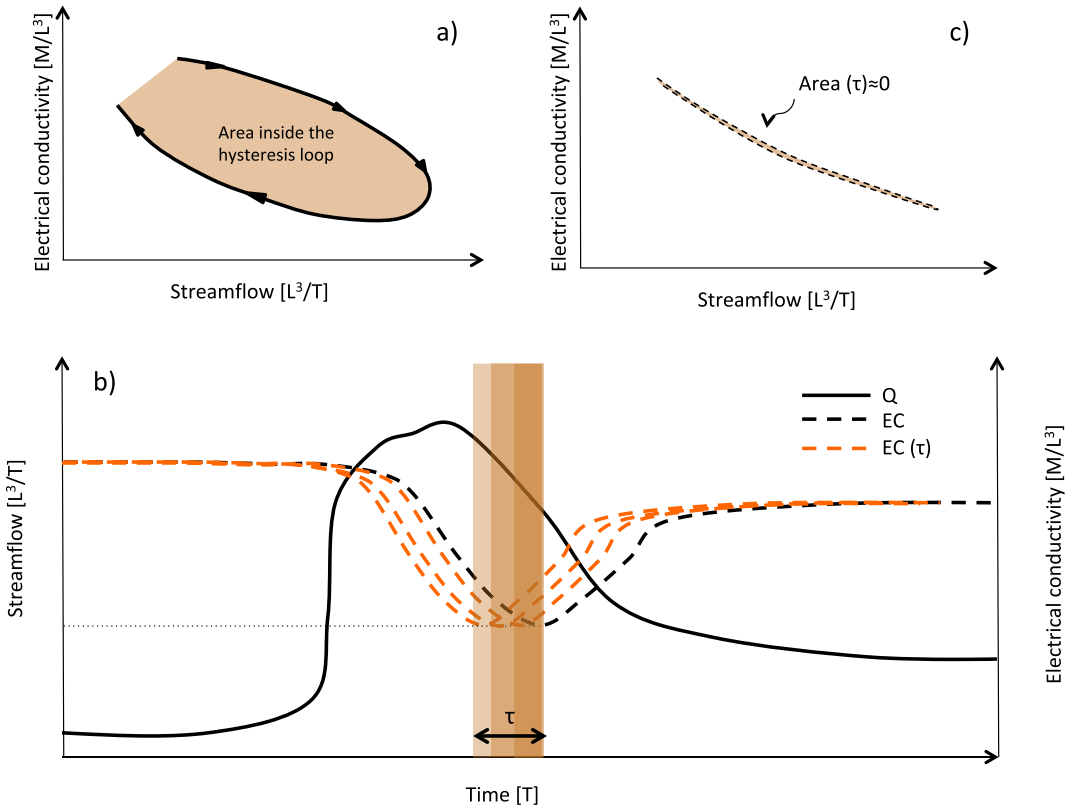

Fig. 4. Conceptual model of new time lag (τ) definition based on the compression of the hysteresis loop between EC and Q during runoff events: a) Theoretical hysteresis loop (clockwise direction) between EC and Q; b) Shifting of EC time series considering a time lag $\tau = 1,2,\ldots,n$ (hours); c) Compression of hysteresis loop using ideal τ value for which the area tends to zero.

3. Results

3.1. Uncertainty analysis of streamflow separation

Two-component hydrograph separation was performed on event R0 using three different tracers: *EC*, δD and $\delta^{18}O$. Data collected during the event are shown in Fig. 5: water discharge *Q* is represented with a solid black line, EC with a dashed blue line, whereas δD and $\delta^{18}O$, at a 4 h time step, are shown with black triangles and red circles, respectively.

As the event proceeds, streamwater becomes more enriched of heavier stable isotopes, i.e., δD and $\delta^{18}O$ become larger, with the arrival of event water. Notice that peak values for δD and $\delta^{18}O$ are delayed with respect to Q. As expected, *EC* is high under baseflow conditions, and then it reduces gradually since the onset of the event to reach a minimum in the first part of the recession limb. Successively, *EC* rises again reaching values similar to the pre-event condition, when event water no longer contributes to streamflow.

The maximum contribution to streamflow from the event component (f_e) is of 0.78 ± 0.016, 0.89 ± 0.09 and 0.9 ± 0.1, when estimated using EC, δD or $\delta^{18}O$, respectively (Table 2). Bear in mind that while *EC* values are hourly, for the case of δD and $\delta^{18}O$ the time interval corresponds to the sampling interval, i.e. 4 h, therefore f_e can be observed at different time steps depending on the tracer. While for the stable isotopes standard deviation is the same for all the three terms of Eq. (4), this is not the case for *EC*, whose standard deviations are the same for C_p and C_{str}, but both differ with respect to that of C_e, which is measured with a different instrument (see section 2.4). Table 2 shows that most of the uncertainty affecting f_e at the peak originates from streamwater, followed by event water, which is lower for the case of EC with respect to stable isotopes. Notice that here uncertainty in f_e is represented by the 95% confidence interval, defined as $\pm 2\ W_{fe}$. Fig. 6 shows event water component at the 5% confidence level under the hypothesis that f_e is normally distributed, i.e., $Q_{str}\,[f_e(i) \pm 2\ W_{f_e}(i)]$. The grey continuous line depicts the streamflow signal whereas the symbols indicate the

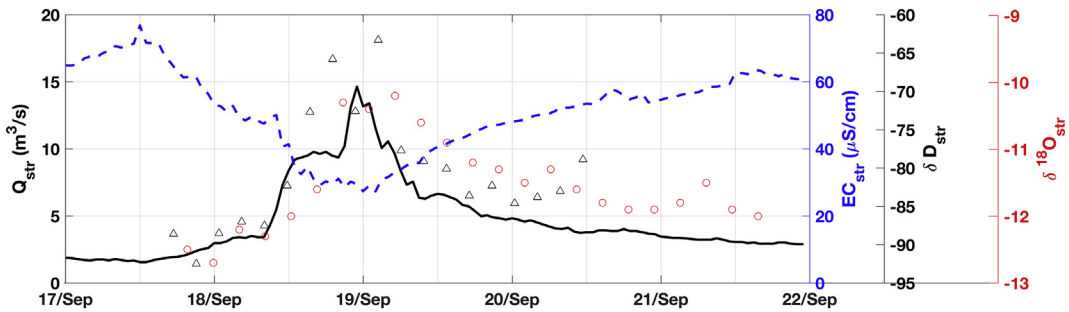

Fig. 5. Water discharge (black solid line), *EC* (blue dashed line), δD(black triangles) and $\delta^{18}O$ (red circles) measured at P2 during the event R0.

Table 2
Tracer data and uncertainty quantification for event R0, computed by the two-component hydrograph separation method.

	EC	δD	$\delta^{18}O$
C_e [μS/cm, ‰]	8.0	−60.0	−10.0
C_p [μS/cm, ‰]	95.0	−90.55	−12.6
Number of streamwater samples	120	19	23
Mean C_{str} [μS/cm, ‰]	51.76	−80.73	−11.54
Standard deviation	0.5% + 1 μS/cm[a], 1 μS/cm[c]	2‰[b]	2‰[b]
Max f_e	0.78 ± 0.016	0.89 ± 0.09	0.9 ± 0.1
f_p[d]	0.22 ± 0.016	0.11 ± 0.09	0.1 ± 0.1
Uncertainty in f_e or f_p accounted for [%][d]:			
Event	30.20	44.02	45.86
Pre-event	5.35	0.65	0.32
Streamwater	64.45	55.33	53.82

[a] Standard deviation of C_{str} and C_p with EC as tracer defined by the Aqua TROLL 200 user's manual.
[b] Standard deviation for C_p, C_e and C_{str} using δD and $\delta^{18}O$, respectively.
[c] Standard deviation of C_e with EC as tracer.
[d] Estimated at the time at which f_e reaches its maximum.

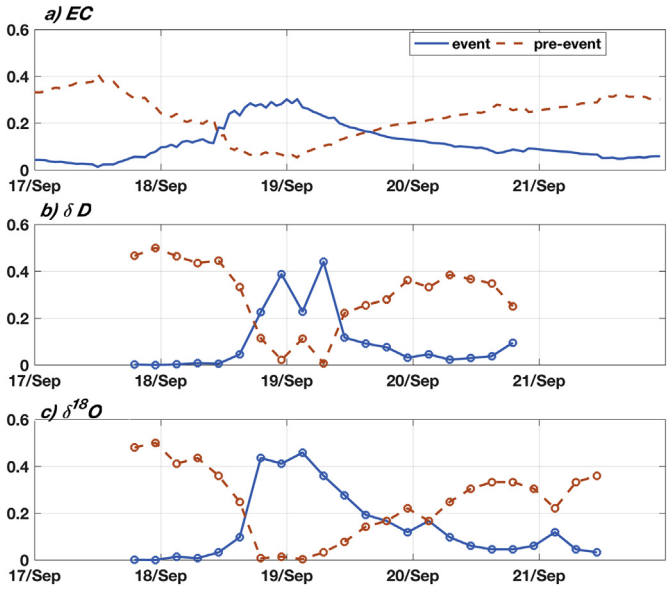

Fig. 7. Percentage of uncertainty corresponding to event (blue continuous line) and pre-event (orange dashed line) water accounted for in f_e when using: a) *EC*, b) *δD* or c) $\delta^{18}O$ as tracers.

fraction of event water obtained by using *EC* (blue circles), *δD* (black squares), and finally $\delta^{18}O$ (red triangles). Error bars indicate the 95% interval of confidence, which is significantly smaller when streamflow separation is performed by using *EC* instead of the stable isotopes, in particular during both the rising and recession limbs.

Given that uncertainty stemming from streamwater, and expressed by the third term of Eq. (4), is nearly the same for all the tracers, we focus on the differences in uncertainty originating from pre-event and event waters, i.e. fromC_p and C_e. Fig. 7 shows that the relative contribution of the different sources of uncertainty is not constant during the event. Before the onset of the event, uncertainty in f_e is chiefly due to uncertainty in C_p because pre-event water accounts for more than half of the mixture. As the event proceeds, the uncertainty stemming from C_p gradually decreases while that stemming from C_e increases since event water accounts for more than half of the mixture at this point, until water discharge peaks at its maximum value. During the recession limb, uncertainty from C_e decreases while that from C_p increases again, since during recession the relative contribution of pre-event water increases again.

3.2. Streamflow and tracer response during the selected events

Fig. 8 shows data recorded during the 8 runoff events presented in section 2.3 (see details in Table 1). Each panel corresponds to an event, grey bars indicate rainfall records, blue and red continuous lines depict *Q* and *EC*, respectively. Notice that regardless the magnitude of precipitation, the increase in *Q*, which maximum is at least two times the baseflow in most of the cases, is followed by a significant reduction of *EC*, which can be attributed to the mixing between new and old water since the former is characterized by lower EC values, i.e., EC_e=8μS/cm.

A better understanding of the *EC*-*Q* relationship during a rainfall event can be gained by inspecting the Fig. 9 which shows *EC* versus *Q* for all the events. Time is marked by the colour of the symbols turning from blue, at the beginning of each event, to yellow at the end. All events are characterized by hysteresis, though the loops are different in shape. Events R1, R2 and ROS1, triggered by relatively large precipitations,

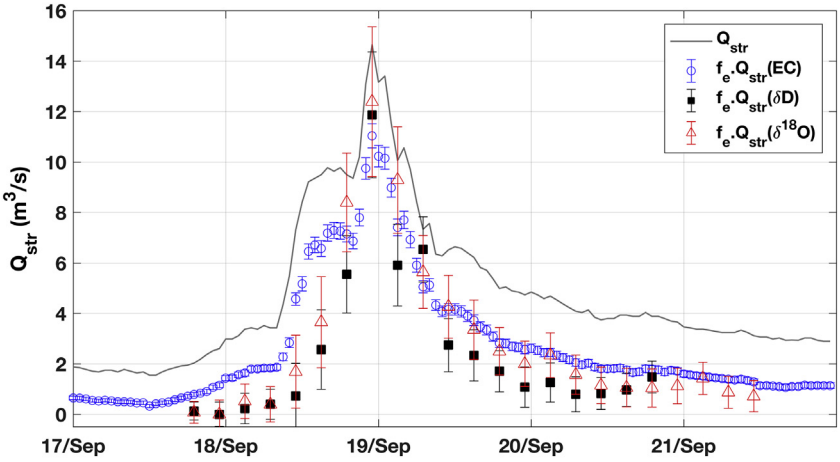

Fig. 6. Identification of event water contribution, including the 95% interval of confidence, for event R0. Grey continuous line shows the streamflow signal and error bars indicate the confidence interval considering a normal distribution for event water component and using: *EC* (blue circles), *δD* (black squares) or $\delta^{18}O$ (red triangles).

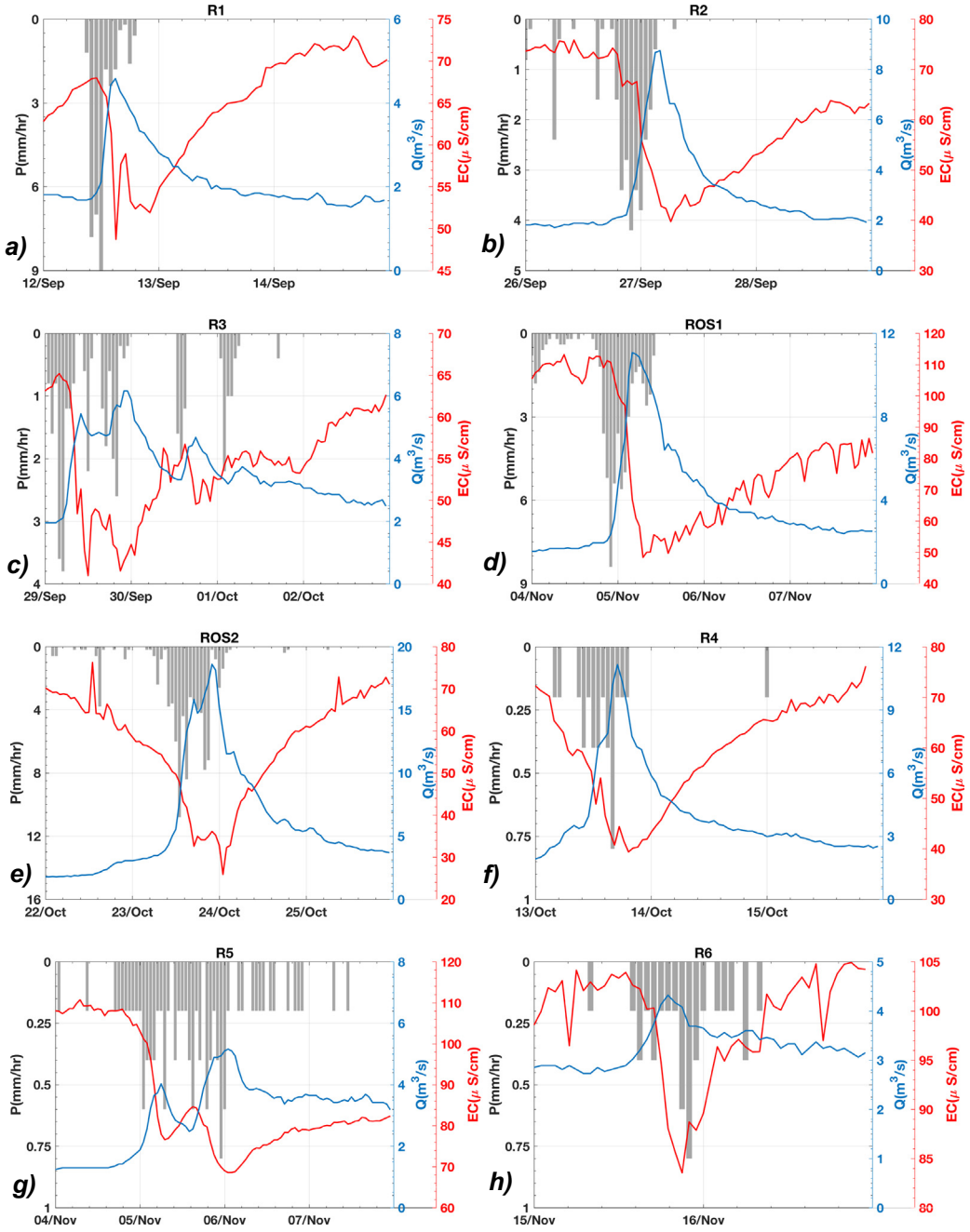

Fig. 8. Time series of precipitation (grey bars), streamflow (blue line) and EC (red line) for each of the 8 runoff events selected during the period 2011–2014.

show wider loops with respect to the others. On the other hand, ROS2 shows a narrow lemniscate loop, even though it has been triggered by the largest precipitation input over the observation period. R5 was split into two parts, i.e., R5a and R5b, since the various blocks of storms generating the runoff produced two well defined peaks (Fig. 8g) and likewise two consecutive hysteresis cycles.

3.3. Time lag estimation and compression of hysteresis loops

We estimated the time lag τ between *EC* and *Q* either as τ_{peak} and $\tau_{50\%}$ and by collapsing the *EC*-*Q* loop with the minimum area criterium described in section 2.5. Results of the last method are shown in Fig. 10, with the original $EC(t)$-$Q(t)$ relationship depicted by grey circles and the translated one, i.e., $EC(t+\tau) - Q(t)$, by orange stars.

The collapse of the loops can be observed in all cases and the proposed methodology was particularly successful in the presence of well-defined hysteresis loops such as for the events R1, R2, ROS1, R4, R5a and R5b. Although the computed τ values slightly differ depending on the definition adopted (see Table 3), considering the associated uncertainty, i.e., $\tau = \pm$ 1 h, results are consistent among methods. In general, larger values were obtained by using the minimum area method here proposed, with the largest difference observed in the case of event ROS1.

Moreover, when confronting the behaviour of τ with respect to the variations in snow depth observed during each event (see Fig. 11), we can see that τ remains nearly constant around 2 h when $\Delta SD \geq 0$, i.e., whenever snow accumulation occurred, whereas when $\Delta SD < 0$, i.e., during snow-melting, τ increased up to 5 h.

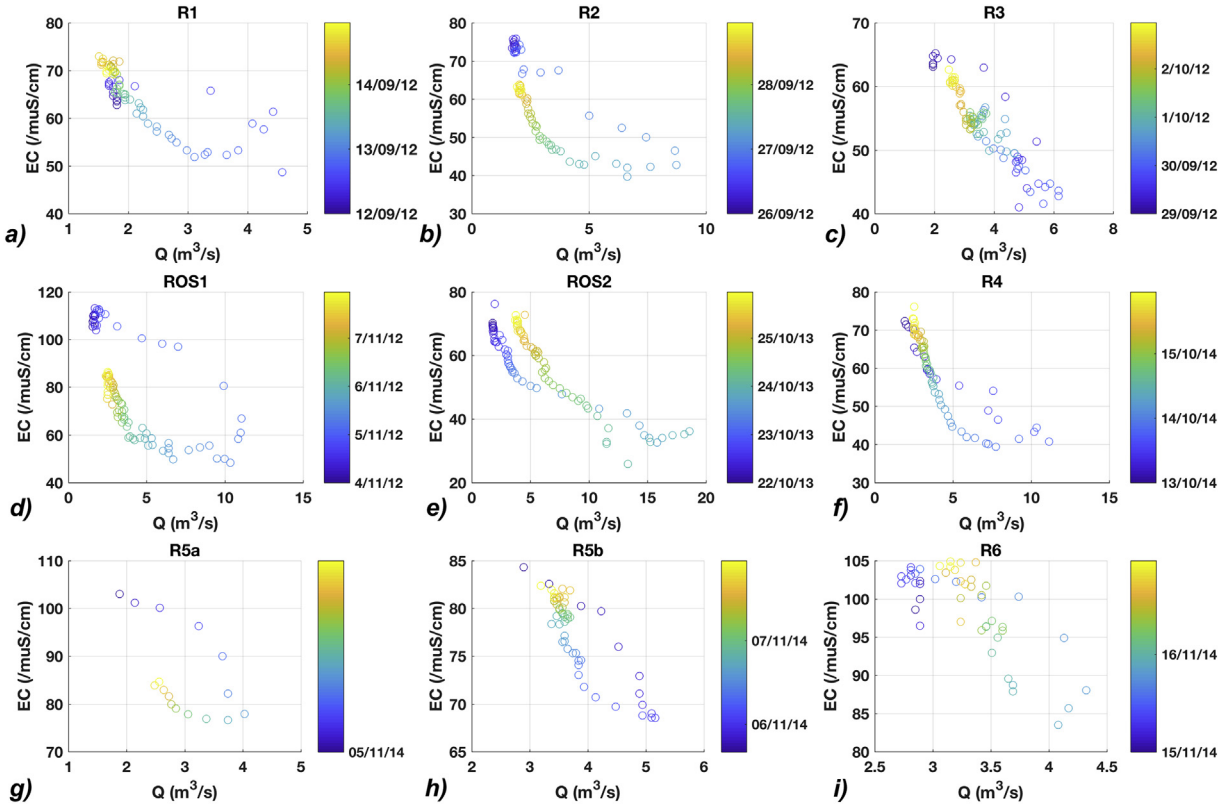

Fig. 9. *EC-Q* relationship characterized by hysteresis loops during each event. The colour of the circles represents the time at which the measurement was taken and it goes from blue (beginning of the event) to yellow (end of the event).

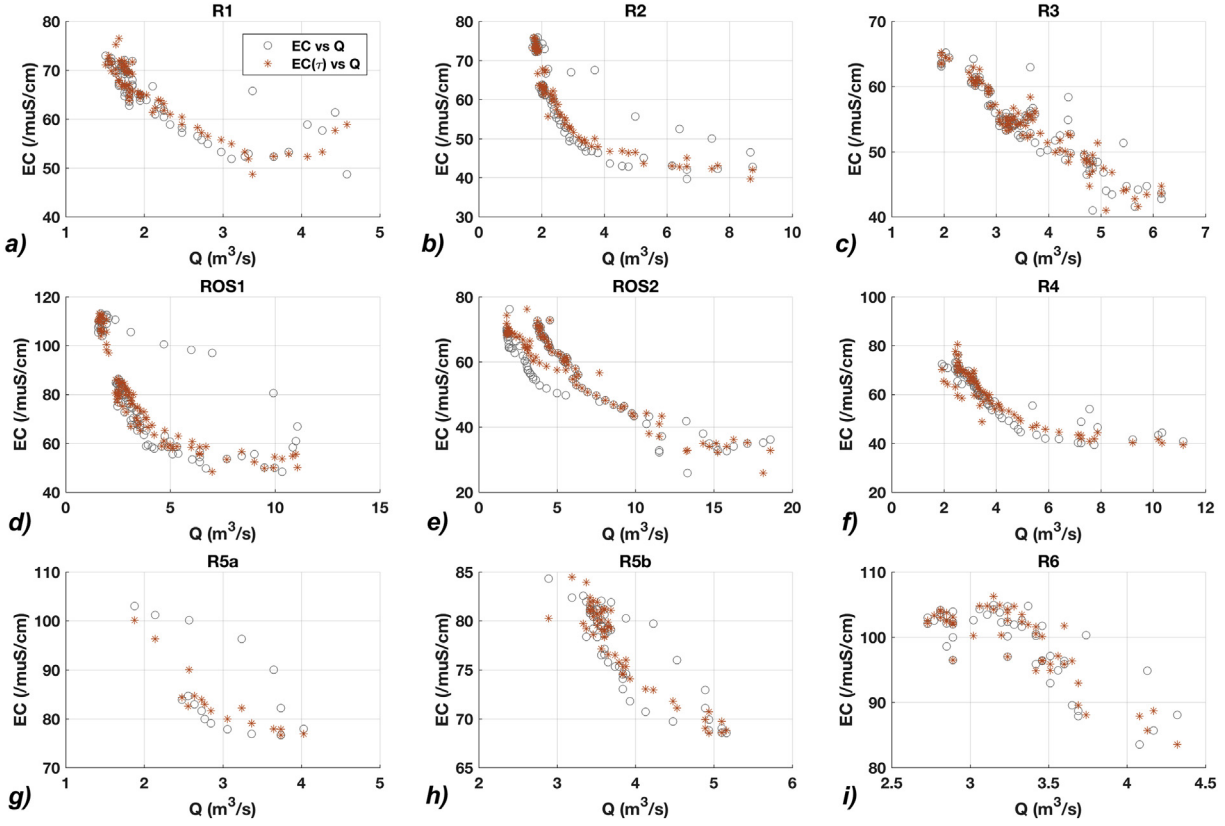

Fig. 10. Comparison between original $EC(t)$-$Q(t)$ relationship for each event (grey circles) and that obtained after translating the EC signal by the time lag τ, i.e., by reporting $EC(t+\tau)$ against $Q(t)$ (orange stars).

Table 3
Time lag (hours) computed between EC and Q using three different definitions.

Event	τ_{peak}	$\tau_{50\%}$	τ
R1	0	1	2
R2	2	3	3
R3	1	1	1
ROS1	3	2	5
ROS2	3	2	3
R4	3	2	3
R5a	1	1	2
R5b	0	1	2
R6	2	2	2

3.4. Streamflow prediction using EC

The relationship between *EC* and *Q* has been investigated in proglacial systems by Gurnell and Fenn (1985) and more recently Weijs et al. (2013) suggested to use *EC* as a proxy of *Q* in alpine streams. With the objective of further exploring this possibility offered by the *EC* signal, we applied the four models presented in the Section 2.6 to the time series of water discharge of the Vermigliana river reported in Section 2.2.

We started by fitting the empirical laws (6), (7) and (8) proposed in the literature to the hourly data of water discharge collected in the period 2012–2014. The resulting models are shown in Fig. 12a with observations represented by open circles and the models by continuous and dashed lines. Although all the three empirical laws capture the mean behaviour of increasing *EC* as *Q* reduces, they are unable to capture the rather broad variability, particularly at high values of *Q*. This drawback of the commonly used empirical relationships is more clearly evidenced in Fig. 13a–c showing the predicted water discharge versus the measured one. A clear bias, leading to a severe underestimation of moderate to high water discharge, is observed for all the empirical laws (6), (7) and (8).

Inspection of the data revealed a seasonal variability of *EC*, which is partially responsible of the dispersion shown in Fig. 12a, given that comparable *EC* values are coupled to widely variable *Q* values in different seasons. To account for this variability we propose to use the expression (9), which is a generalization of the power law model (6) for a seasonally variable *EC*. The period *T* characterizing the seasonal variability of *EC* has been set to $T = 4380$ h $= 182.5$ days, while the other parameters are obtained by fitting expression (9) to the recorded *Q* (see Table 4). Fig. 12b shows that the additional degree of freedom included by allowing *EC* to vary seasonally leads to a better reproduction of the variability in the relationship between *Q* and *EC*, which eliminates the bias introduced by the previous relationships. This is evidenced in Fig. 13d showing the predicted water discharge by the model (9) versus the observed one.

Given that the above four models are characterized by a different number of parameters, and to support the visual inspection of the Figs. 12a–b and 13a–d, we computed the AIC (Akaike Information Criterion) scores as $AIC = 2k + Nln(RSS)$, where k is the number of free parameters, N the number of observations and $RSS = \sum_{i=1}^{N}[Q_{str}(t_i) - \hat{Q}_{str}(t_i)]^2$ is the sum of the squared residuals. Here $\hat{Q}_{str}(t_i)$ is the measured water discharge at time t_i. The Akaike score penalizes models with a larger number of parameters, which are expected to provide larger values of R^2 even in the absence of a better predictivity. Table 4 shows that the transient model is the one with the smallest AIC and the largest R^2, thereby confirming the visual impression gained from Figs. 12 and 13 of a better reproduction of experimental data by the model (9).

Fig. 14 shows how the model (9) reproduces the eight selected runoff events presented in Section 2.3. We applied the model by using the recorded *EC* during the events as predictive variable and its translation with the time lag suggested for each event by the hysteresis analysis presented in Section 2.5. In all cases delaying *EC* by a time lag τ improves predictability of the model, i.e. the computed water discharge is in better agreement with the observed one. All the events, except R6, are captured by the transient model (9), with some of them (i.e., R3, R4 ROS1, ROS2) better reproduced than others, but globally the reproduction is satisfactory.

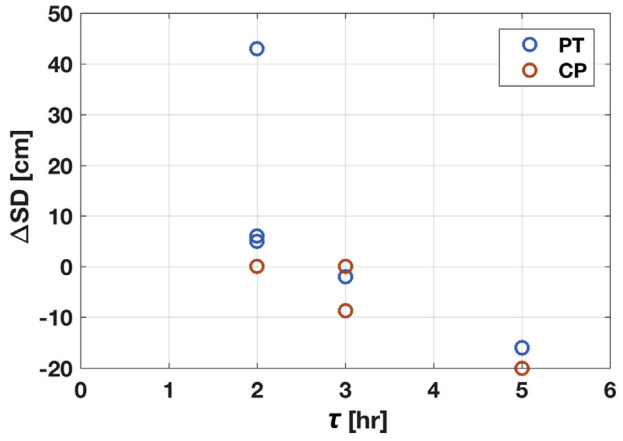

Fig. 11. Observed variation in snow depth (ΔSD against computed τ for the analysed runoff events. Blue open circles correspond to data from Passo del Tonale (PT) station while orange open circles to data from Capanna Presena (CP) station.

4. Discussion

4.1. Use of EC for hydrograph separation and uncertainty quantification

Streamflow separation into event and pre-event components using EC data provided similar results than with stable isotopes (δD and $\delta^{18}O$), with slight differences observed during the rising and falling limbs and likewise at the peak of streamflow. Estimates of event water contribution were affected by a lower measurement uncertainty when performed with EC and given the additional advantage of higher temporal resolution and lower operational cost, using EC to separate the contributions may be preferable than the classical method based on stable isotopes.

As observed in section 3.1, the maximum contribution to streamflow from event water is higher (i.e., of about 10%) when estimated by stable isotopes (δD or $\delta^{18}O$) than with EC (Table 2). Yet, a closer inspection of Fig. 6 shows, on one hand, that EC provides higher estimates, in comparison to stable isotopes, of event water contribution during the rising and recession limbs of the hydrograph. On the other hand, the interval of confidence of f_e is much smaller when *EC* is used as tracer instead of the stable isotopes (see Fig. 6), in particular before and after water discharge peak. Therefore our results, consistently with previous findings (see e.g., Laudon and Slaymaker, 1997), indicate that also in a mesoscale (<100 km^2) Alpine catchment, we can effectively apply EC to perform hydrograph separation. In particular, results computed using EC information are affected by a lower standard deviation and allow a higher temporal resolution than using stable isotopes. Still we should be aware than under certain conditions EC may behave as a non-conservative, depending on specific geological conditions as evidenced in earlier studies (Hayashi et al., 2012; Laudon and Slaymaker, 1997).

The uncertainty stemming from C_{str} was relatively constant and the most interesting variations were observed in the uncertainties originating from C_p and C_e (Fig. 7). The sensitivity of the total uncertainty of f_e to the first two terms of Eq. (4) varied as the event proceeded with uncertainty due to pre-event water dominating at the onset and the end of the event and that due to event water dominating around the peak.

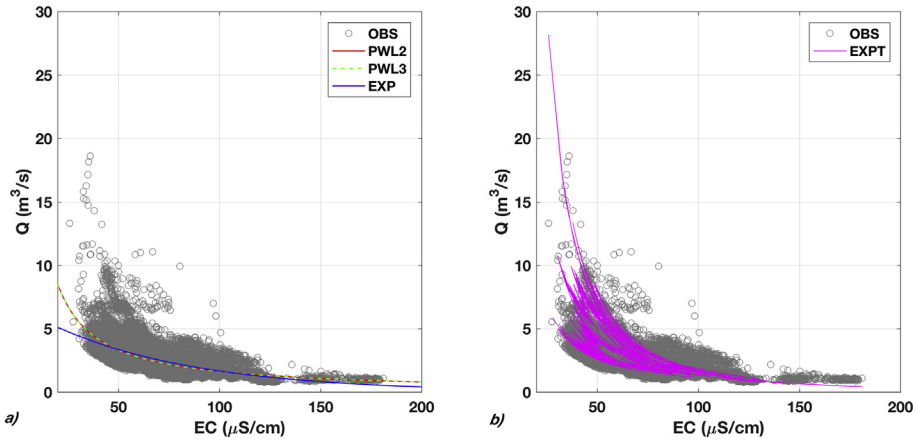

Fig. 12. Experimental data (grey circles) and: a) Power law model with 2 (PWL2) and 3 (PWL3) fitting parameters, exponential model (EXP) and; b) proposed transient model (EXPT).

However, while uncertainty estimated with EC takes into account the initial increase of the portion of the total uncertainty originating from C_e since the onset of the storm, with stable isotopes the first term of Eq. (4) was instead close to zero. Also, the higher resolution of EC measurements allowed a more accurate approximation of the uncertainty and its evolution in time.

4.2. Catchment functioning through the interpretation of hysteresis loops and time lag between EC-Q

The hysteresis observed between Q and EC in all events (Fig. 9) evidenced the existence of a time delay between streamflow and EC in response to the precipitation input. Time lag between natural tracers (e.g., dissolved solutes and EC) and water discharge is typically estimated as the shift in time between the (positive) peak of *Q* and the following minimum of *EC* (τ_{peak}) or the shift between 50% of the rise in *Q* and the 50% decline of *EC* ($\tau_{50\%}$). However, both methods have limitations related to data resolution and the oscillations of field measurements. The first may affect the correct identification of peak values, while the second may hamper the identification of the time at which EC starts to reduce. We proposed a new method to compute the time lag, τ, as the shift in EC time series needed to make the hysteresis loop between EC and Q at the event scale as small as possible (Eq. (5)). The interpretation of the time lag is helpful to better understand the hydrological functioning of the catchment.

Estimates of the time lag, obtained by translating the *EC* time series until the observed hysteresis loop is compressed (Fig. 10), were equal or slightly higher than those computed by using the other definitions (Table 3), with the highest value, i.e., τ=5 h, obtained for the event ROS1. Given the particular nature of this event, i.e., rain-on-snow, the

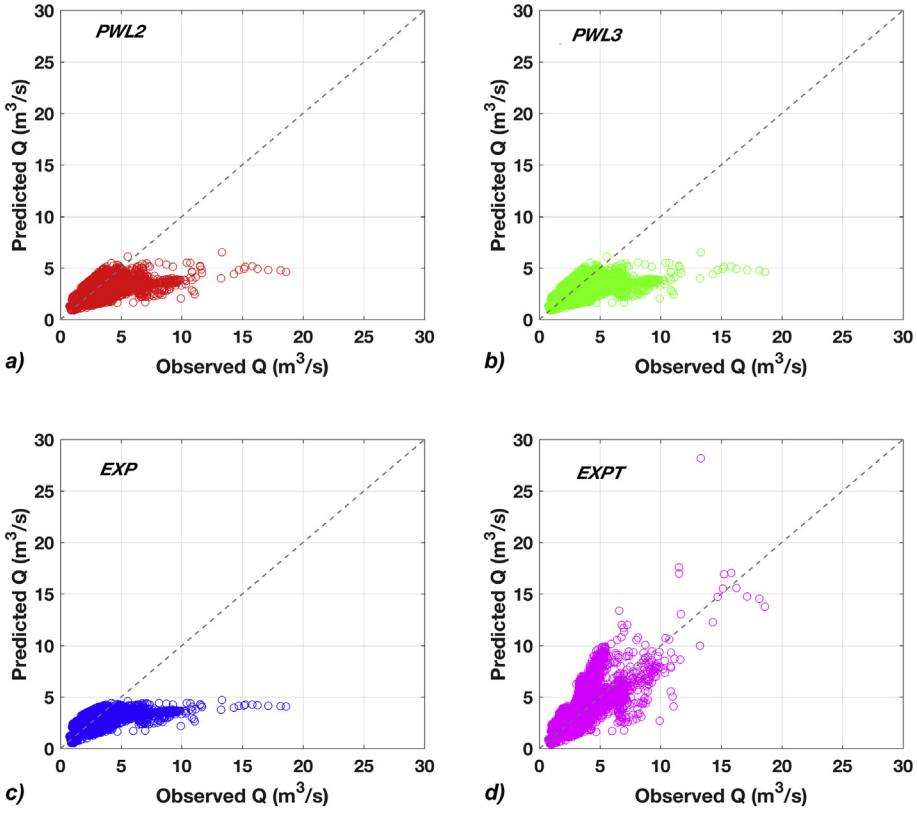

Fig. 13. Comparison between observed and predicted values of *Q* for each model.

Table 4
Model fitting parameters, number of free parameters k, R^2 coefficients and AIC scores.

	a	b	c	d	T(hr)	k	R^2	AIC
PWL2	186.8	−1.03	–	–	–	2	0.4414	125010
PWL3	185.7	−1.028	−0.005	–	–	3	0.4414	125010
EXP	6.774	−0.01405	–	–	–	2	0.4290	125220
EXPT	−1.8	−5.06	−0.54	1/2	4380	5	0.5553	121800

larger value of τ can be explained as the result of changes in the storage of water in the snowpack, causing further dilution due to snow-melting in addition to rainfall. The previous statement was verified by confronting the behaviour of τ with respect to the variations in snow depth observed during each event (Fig. 11), with showed consistency between data from two different meteorological stations. Essentially, during snow accumulation τ remains constant and equal to 2 h, instead during snow-melting it increases as an effect of the storage of the melted water into the snowpack. In this situation τ increased up to 5 h in the events considered in this work. This outcome is not observed with the other definitions as time lag estimates were lower and less variable, which suggests that the method here proposed is able to indicate the occurrence of storage of water into the snowpack and snow-melting during events and thus provide a more accurate time lag estimate in the presence of snow-melting.

4.3. Water discharge estimates by means of calibrated functional relationships between EC and water discharge

Four models were applied to available data using EC as a proxy of water discharge: three based on empirical relationships proposed in the literature (power law and exponential) and a fourth by adopting a generalization of the power law model, which includes seasonal variability of the relationship between *Q* and *EC*.

All models were evaluated in terms of both the coefficient of determination R^2 and the Akaike scores (see Table 4), since the former indicates the fraction of the variance of the *Q* signal that can be explained by *EC*, while the latter provides an indication of model's quality, penalizing the models with a larger number of fitting parameters. The optimal model (Eq. (9)), eliminates the bias that characterizes the other models, which underestimate median to high water discharges. Moreover, this model was applied to each of the 8 runoff events identified during the autumn-winter season and results further verify that the inclusion of the time lag not only improves the estimates of *Q* but also the timing of occurrence of peak values.

In general, all models here investigated underestimate high streamflows, in particular those occurring in spring-summer seasons, which in this period are induced mainly by snow-melting. However, the transient model (Eq. (9)) produces better estimates with respect to the models so far proposed in the literature. For the autumn-winter season, when high flows are mostly caused by extreme rainfall events, water discharge predictions improved thanks to the inclusion of the time lag, although the model (Eq. (9)) was not effective for all the runoff events since a tendency to underestimate high flows were observed in some of the events.

Our analysis evidenced the need for further research aimed at identifying other type of constraints in the modelling framework able to solve this prominent issues, possibly considering additional explanatory variables to EC into the models explored in this work.

5. Conclusions

This work shows how continuous monitoring of EC in Alpine headwaters can be useful for multiple purposes such as hydrograph separation, understanding of catchment functioning through the interpretation of hysteresis loops, and water discharge prediction by means of calibrated functional Q-EC relationships. This multi-purpose approach and the ease of use and acquisition of EC data make EC time series a precious resource both for the understanding of hydrological processes and the solution of practical problems such as the estimation of river discharge in Alpine catchments, where the construction of

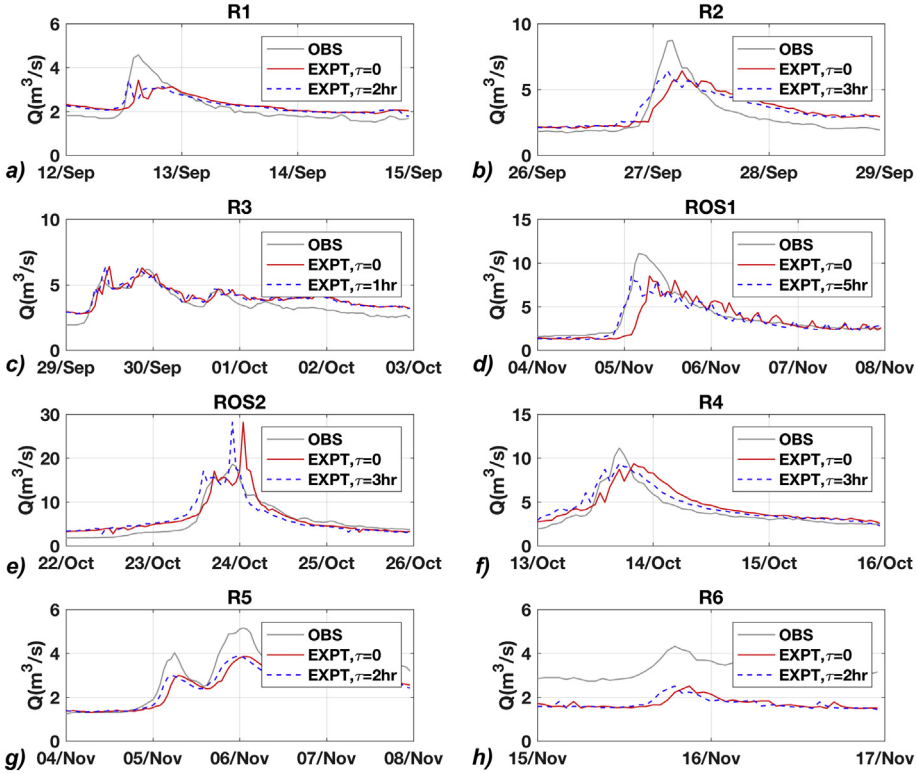

Fig. 14. Prediction of *Q* using *EC* as proxy for each of the 8 runoff events selected during the period 2012–2014.

proper gauging stations may be unfeasible. This long term monitoring with hourly frequency is only possible with other tracers at very high costs and makes EC time series an unique source of information. Our results are particularly relevant for Alpine environments, where a marked difference between EC and residence time of different water sources exists. In other contexts, complex biochemical and hydrogeochemical processes should be carefully considered. As long term EC time series will become more common, including physically based modeling of EC time series will be beneficial to improve hydrological models and the collected EC data could be used to better constrain the models considering also the coupled interaction between hydrology and geochemistry.

Acknowledgements

This research was partially supported by the European Communities Seventh Framework Programme under grant agreement no. 603629-ENV-2013-6.2.1-Globaqua. We would also like to acknowledge Agostino Tonon and Federica Camin from the Edmund Mach Foundation (San Michele dell'Adige, Trento - Italy) for the stable isotope laboratory analyses. G.C. acknowledges the support of the Stiftungsfonds für Umweltökonomie und Nachhaltigkeit GmbH (SUN) and likewise the support from the DFG (Deutsche Forschungsgemeinschaft) Research Group FOR2793/1)"Sensitivity of High Alpine Geosystems to Climate Change since 1850 (SEHAG)" (grant CH981/3-1). The meteorological survey of the Autonomous Province of Trento is acknowledged for the public availability of the collected meteorological data.

References

Barberá, J., Jódar, J., Custodio, E., González-Ramón, A., Jiménez-Gavilán, P., Vadillo, I., Pedrera, A., Martos-Rosillo, S., 2018. Groundwater dynamics in a hydrologically-modified alpine watershed from an ancient managed recharge system (Sierra Nevada national park, southern Spain): insights from hydrogeochemical and isotopic information. Sci. Total Environ. 640, 874–893.

Behrens, H., Bergmann, H., Moser, H., Rauert, W., Stichler, W., Ambach, W., Eisner, H., Pessl, K., 1971. Study of the discharge of alpine glaciers by means of environmental isotopes and dye tracers. Zeitscherkd Glazialgeo 7, 79–102.

Benettin, P., van Breukelen, B.M., 2017. Decomposing the bulk electrical conductivity of streamflow to recover individual solute concentrations at high frequency. Environmental Science & Technology Letters 4 (12), 518–522.

Bolto, B., Hoang, M., Xie, Z., 2012. A review of water recovery by vapour permeation through membranes. Water Res. 46 (2), 259–266.

Brown, L.E., Hannah, D.M., Milner, A.M., Soulsby, C., Hodson, A.J., Brewer, M.J., 2006. Water source dynamics in a glacierized alpine river basin (Taillon-gabiétous, French pyrénées). Water Resour. Res. 42 (8).

Callegari, E., Dal Piaz, G., nazionale delle ricerche (Italia), C, 1973. Field Relationships between the Main Igneous Masses of the Adamello Intrusive Massif (Northern Italy). Società cooperativa tipografica.

Chiogna, G., Santoni, E., Camin, F., Tonon, A., Majone, B., Trenti, A., Bellin, A., 2014. Stable isotope characterization of the Vermigliana catchment. J. Hydrol. 509, 295–305.

Chiogna, G., Majone, B., Paoli, K.C., Diamantini, E., Stella, E., Mallucci, S., Lencioni, V., Zandonai, F., Bellin, A., 2016. A review of hydrological and chemical stressors in the Adige catchment and its ecological status. Sci. Total Environ. 540, 429–443.

Collins, D.N., 1979. Hydrochemistry of meltwaters draining from an alpine glacier. Arct. Alp. Res. 307–324.

Engel, M., Penna, D., Bertoldi, G., Dell'Agnese, A., Soulsby, C., Comiti, F., 2015. Identifying runoff contributions during melt-induced runoff events in a glacierized alpine catchment. Hydrol. Process. 343–364.

Engel, M., Penna, D., Bertoldi, G., Vignoli, G., Werner, T., Comiti, F., 2018. Controls on spatial and temporal variability of streamflow and hydrochemistry in a glacierized catchment. Hydrological Earth System Sciences 1–59.

Evans, C., Davies, T.D., 1998. Causes of concentration/discharge hysteresis and its potential as a tool for analysis of episode hydrochemistry. Water Resour. Res. 34 (1), 129–137.

Genereux, D., 1998. Quantifying uncertainty in tracer-based hydrograph separations. Water Resour. Res. 34 (4), 915–919.

Glover, B., Johnson, P., 1974a. Variations in the natural chemical concentration of river water during flood flows, and the lag effect. J. Hydrol. 22 (34), 303–316.

Glover, B., Johnson, P., 1974b. Variations in the natural chemical concentration of river water during flood flows, and the lag effect. J. Hydrol. 22 (3-4), 303–316.

Gurnell, A., Fenn, C., 1985. Spatial and temporal variations in electrical conductivity in a pro-glacial stream system. J. Glaciol. 31 (108), 108–114.

Hayashi, M., Vogt, T., Mächler, L., Schirmer, M., 2012. Diurnal fluctuations of electrical conductivity in a pre-alpine river: effects of photosynthesis and groundwater exchange. J. Hydrol. 450, 93–104.

Herms, I., Jódar, J., Soler, A., Vadillo, I., Lambán, L., Martos-Rosillo, S., Núñez, J., Arnó, G., Jorge, J., 2019. Contribution of isotopic research techniques to characterize high-mountain-Mediterranean karst aquifers: the Port del Comte (eastern Pyrenees) aquifer. Sci. Total Environ. 656, 209–230.

Jódar, J., Custodio, E., Lambán, L.J., Martos-Rosillo, S., Herrera-Lameli, C., Sapriza-Azuri, G., 2016. Vertical variation in the amplitude of the seasonal isotopic content of rainfall as a tool to jointly estimate the groundwater recharge zone and transit times in the Ordesa and Monte Perdido national park aquifer system, North-Eastern Spain. Sci. Total Environ. 573, 505–517.

Jódar, J., Cabrera, J.A., Martos-Rosillo, S., Ruiz-Constán, A., González-Ramón, A., Lambán, L.J., Herrera, C., Custodio, E., 2017. Groundwater discharge in high-mountain watersheds: a valuable resource for downstream semi-arid zones. The case of the Bérchules river in Sierra Nevada (southern Spain). Sci. Total Environ. 593, 760–772.

Kuhn, M., Batlogg, N., 1998. Glacier runoff in alpine headwaters in a changing climate. International Association of Hydrological Sciences, Publication 248, 79–88.

Laudon, H., Slaymaker, O., 1997. Hydrograph separation using stable isotopes, silica and electrical conductivity: an alpine example. J. Hydrol. 201 (1), 82–101.

Majone, B., Villa, F., Deidda, R., Bellin, A., 2016. Impact of climate change and water use policies on hydropower potential in the south-eastern alpine region. Sci. Total Environ. 543, 965–980.

Merz, R., Blöschl, G., 2003. A process typology of regional floods. Water Resour. Res. 39 (12).

Meteotrentino, 2011. Evoluzione e monitoraggi recenti dei ghiacchiai trentini. Meteorological Office of the Trentino Province.

Penna, D., Engel, M., Mao, L., Dell'Agnese, A., Bertoldi, G., Comiti, F., 2014. Tracer-based analysis of spatial and temporal variation of water sources in a glacierized catchment. Hydrol. Earth Syst. Sci. Discuss. 11 (5), 4879–4924.

Penna, D., van Meerveld, H., Zuecco, G., Dalla Fontana, G., Borga, M., 2016a. Hydrological response of an alpine catchment to rainfall and snowmelt events. J. Hydrol. 537, 382–397.

Penna, D., Zuecco, G., Crema, S., Trevisani, S., Cavalli, M., Pianezzola, L., Marchi, L., Borga, M., 2016b. Response time and water origin in a steep nested catchment in the Italian dolomites. Hydrol. Process. 31 (4), 768–782 (pages n/a–n/a. HYP-16-0376.R1).

Piccolroaz, S., Majone, B., Palmieri, F., Cassiani, G., Bellin, A., 2015. On the use of spatially distributed, time-lapse microgravity surveys to inform hydrological modeling. Water Resour. Res. 51 (9), 7270–7288.

Pinder, G.F., Jones, J.F., 1969. Determination of the ground-water component of peak discharge from the chemistry of total runoff. Water Resour. Res. 5 (2), 438–445.

Singh, P., Spitzbart, G., Hübl, H., Weinmeister, H., 1997. Hydrological response of snowpack under rain-on-snow events: a field study. J. Hydrol. 202 (1), 1–20.

Sklash, M.G., Farvolden, R.N., 1979. The role of groundwater in storm runoff. Dev. Water Sci. 12, 45–65.

Stewart, I.T., 2009. Changes in snowpack and snowmelt runoff for key mountain regions. Hydrol. Process. 23 (1), 78–94.

Surfleet, C.G., Tullos, D., 2013. Variability in effect of climate change on rain-on-snow peak flow events in a temperate climate. J. Hydrol. 479, 24–34.

Walling, D., Foster, I., 1975. Variations in the natural chemical concentration of river water during flood flows, and the lag effect: some further comments. J. Hydrol. 26 (3–4), 237–244.

Walling, D., Webb, B., 1980. The spatial dimension in the interpretation of stream solute behaviour. J. Hydrol. 47 (1–2), 129–149.

Walling, D., Webb, B., 1986. Solutes in river systems. Solute Processes, pp. 251–327.

Weijs, S.V., Mutzner, R., Parlange, M.B., 2013. Could electrical conductivity replace water level in rating curves for alpine streams? Water Resour. Res. 49 (1), 343–351.

Zuecco, G., Penna, D., Borga, M., Meerveld, H., 2015. A versatile index to characterize hysteresis between hydrological variables at the runoff event timescale. Hydrol. Process. 30 (9), 1449–1466.